Multinucleon transfer in ^{58}Ni + ^{60}Ni and ^{60}Ni + ^{60}Ni in a stochastic mean-field approach

B. Yilmaz,[1] S. Ayik,[2] O. Yilmaz,[3] and A. S. Umar[4]
[1]*Physics Department, Faculty of Sciences, Ankara University, 06100 Ankara, Turkey*
[2]*Physics Department, Tennessee Technological University, Cookeville, Tennessee 38505, USA*
[3]*Physics Department, Middle East Technical University, 06800 Ankara, Turkey*
[4]*Department of Physics and Astronomy, Vanderbilt University, Nashville, Tennessee 37235, USA*

(Received 24 July 2018; published 7 September 2018)

The multinucleon exchange mechanism in ^{58}Ni + ^{60}Ni and ^{60}Ni + ^{60}Ni collisions is analyzed in the framework of the stochastic mean-field approach. The results of calculations are compared with the time-dependent random-phase approximation (TDRPA) calculations and the recent data of ^{58}Ni + ^{60}Ni. A good description of the data and a relatively good agreement with the TDRPA calculations are found.

DOI: 10.1103/PhysRevC.98.034604

I. INTRODUCTION

The transfer of particles between two reacting nuclei is believed to have a profound impact on the outcome of nuclear reactions. These include the observed reduction in the number of evaporated neutrons from a compound nucleus linked to the excitation of the precompound collective dipole mode [1–5], which is likely to occur when ions have significantly different N/Z ratio, the influence of transfer on fusion particularly at deep sub-barrier energies [6–21] and the distribution of fragments in deep-inelastic and quasifission reactions [22–26]. These reaction aspects are intimately related to the dissipation and equilibration during the early stages of the collision [27–31] and at low energies also depend on the shell structure of the participating nuclei [32–36] and is sensitive to the details of the evolution of the shape of the composite system [37]. This is in contrast to most classical pictures, which generally assume near instantaneous, isotropic equilibration. For these low-energy heavy-ion collisions the relative motion of the centers of the two nuclei is characterized by a short wavelength and thus allows for a classical treatment, whereas the wavelength for the particle motion is not small compared to nuclear sizes and should be treated quantum mechanically. The mean-field approach such as the time-dependent Hartree-Fock (TDHF) theory [38,39] and its extensions provide a microscopic basis for describing the heavy-ion reaction mechanism at low bombarding energies, and have been extensively used to study particle transfer [14,40–48].

In recent work, Williams *et al.* presented an experimental investigation of the nucleon transfer in the ^{58}Ni + ^{60}Ni collisions at center of mass energies in the vicinity of the fusion barrier [49]. They analyzed the experimental data in conjunction with the numerical simulations using TDHF theory and its extension, the time-dependent random-phase approximation (TDRPA) [41,50–52]. At low energies, the TDHF provides a good description of the mean evolution of the nuclear collective motion but fails to describe the fluctuating dynamics of the collective motion. The authors, employing the Balian and Vénéroni formula (it is referred to as TDRPA in [49]), calculated the dispersion of the primary fragment distributions, and obtained a very good agreement with the experimental results. Apparently, due to a technical difficulty of the approach, the authors interpret the experimental data of the ^{58}Ni + ^{60}Ni collisions, with the result of the calculations of the symmetric ^{60}Ni + ^{60}Ni collision at the same $E_{\mathrm{c.m.}}/V_B$ value, where V_B is the corresponding barrier height.

II. THEORETICAL APPROACH

Here, we undertake a study for the same experimental data for the ^{58}Ni + ^{60}Ni system by employing the stochastic mean-field (SMF) approach [53]. The SMF approach goes beyond the mean-field approximation by incorporating the mean-field fluctuations into the description. The approach relies on an ensemble of mean-field events specified with quantal and thermal fluctuations at the initial state. It is possible to project the SMF on macroscopic variables which provide a much easier description of the dissipation and fluctuation mechanism in terms of the relevant macroscopic variables. The relevant macroscopic variables evolve according to the generalized Langevin description characterized by a set of quantal transport coefficients. As described in Refs. [54–56], the transport coefficients are determined entirely by the occupied TDHF wave functions. They include quantal effects due to the shell structure, contain the full collision geometry, and involve no adjustable parameters.

III. RESULTS

Here, we perform calculations for the nucleon exchange mechanism for range of impact parameters leading to deep-inelastic collisions. In this case, due to the dinuclear configuration of the collision, the relevant macroscopic variables are the number of neutron and protons on either side of the window plane. Since ^{58}Ni is deformed, we carry out calculations for side and tip configurations of ^{58}Ni nucleus. As an example, Fig. 1 shows the density profile of the ^{58}Ni + ^{60}Ni at the center of mass energy of $E_{\mathrm{c.m.}} = 135.6$ MeV and the

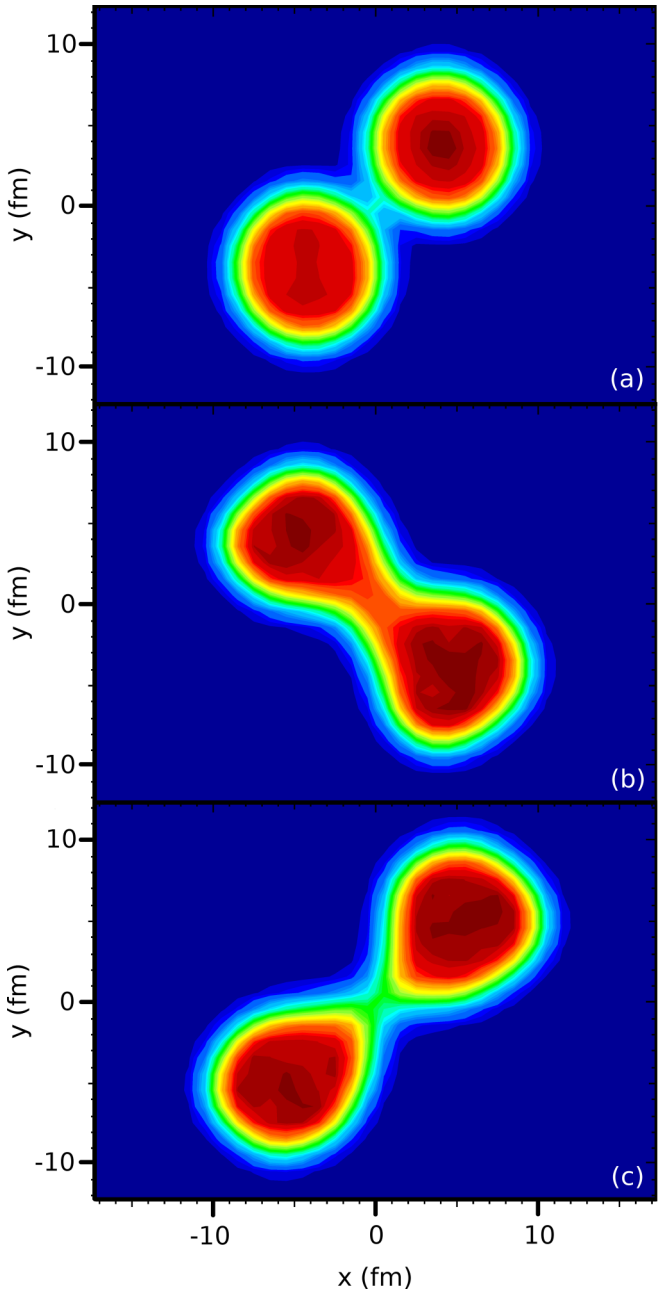

FIG. 1. Density profile of the ^{58}Ni + ^{60}Ni at the center of mass energy $E_{\text{c.m.}} = 135.6$ MeV and the impact parameter $b = 5.2$ fm in the side configuration, at times 300 (a), 750 (b), and 1250 fm/c (c).

impact parameter $b = 5.2$ fm for the initial side orientation of ^{58}Ni, at times 300, 750, and 1250 fm/c. The dynamical symmetry axis of the dinuclear system is determined by the principle axis of the mass quadrupole moment tensor. The window plane is perpendicular to the symmetry axis and passing through the minimum density slice. The neutron and proton numbers on one side of the dinuclear system (we refer to as projectile-like fragment) is determined by integrating the local density on one side of the window plane. From the Langevin equations of the neutron N^λ and proton Z^λ numbers of the projectile-like fragments in each event,

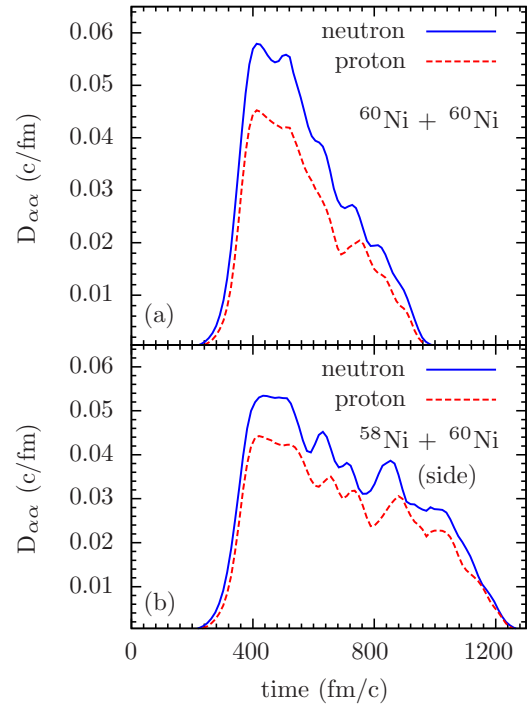

FIG. 2. Neutron (solid lines) and proton (dotted lines) diffusion coefficients at the center of mass energy $E_{\text{c.m.}} = 135.6$ MeV and the impact parameter $b = 5.2$ fm in ^{60}Ni + ^{60}Ni collisions (a) and in ^{58}Ni + ^{60}Ni collisions in the side configuration (b).

we can deduce a set of couple differential equations for the covariances $\sigma^2_{NN}(t) = \overline{(N^\lambda - N)^2}$, $\sigma^2_{ZZ}(t) = \overline{(Z^\lambda - Z)^2}$, and $\sigma^2_{NZ}(t) = \overline{(N^\lambda - N)(Z^\lambda - Z)}$. Here, $N = \overline{N^\lambda}$ and $Z = \overline{Z^\lambda}$ are mean values of the neutron and proton numbers, λ indicates the event label, and the bar denotes the average over the ensemble generated in the SMF simulations. The coupled differential equations for the covariances are given by Eqs. (17)–(19) in Ref. [55], which involve the neutron $D_{NN}(t)$ and proton $D_{ZZ}(t)$ diffusion coefficients and the derivatives of drift coefficients. These sets of coupled equations for covariances are also familiar from the phenomenological nucleon exchange model, and they were derived from the Fokker-Planck equation for the fragment neutron and proton distributions in deep-inelastic heavy-ion collisions [57–59].

For numerical calculations we employ the TDHF code of Umar *et al.* [60,61]. The computations are carried out in a box with size of $70 \times 30 \times 50$ fm^3. The initial separation of the nuclei is taken as 30 fm. The SLy4d [62] Skyrme interaction is used. We evaluate the diffusion coefficients using Eq. (37) in Ref. [55] and determine the derivative of the drift coefficients around their mean values from the one-sided drift path as described in Ref. [54]. Figure 2 shows neutron (solid lines) and proton (dotted lines) diffusion coefficients at the center of mass energy $E_{\text{c.m.}} = 135.6$ MeV and the impact parameter $b = 5.2$ fm in ^{60}Ni + ^{60}Ni collisions in the upper panel and in ^{58}Ni + ^{60}Ni collisions in the side configuration in the lower panel. The fluctuations in the behavior of the diffusion coefficients are partly due to the effect of the shell structure and

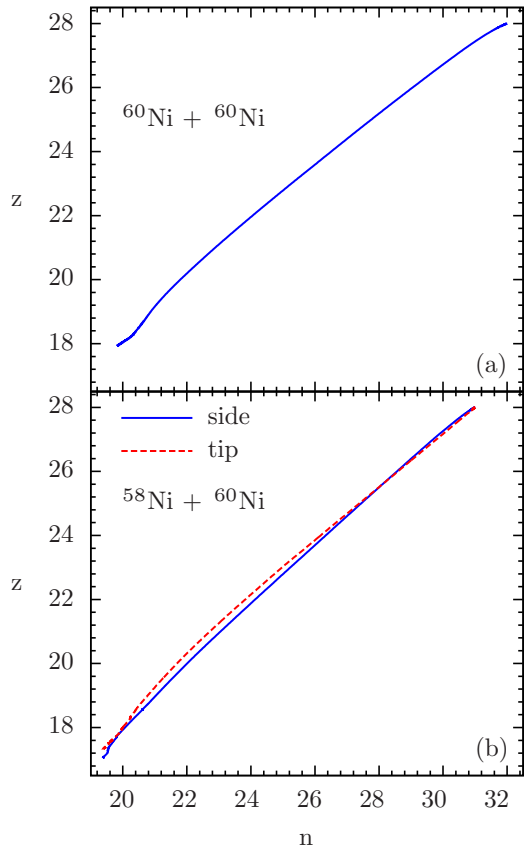

FIG. 3. One-sided mean-drift path at the center of mass energy $E_{\text{c.m.}} = 135.6$ MeV and the impact parameter $b = 5.2$ fm in ^{60}Ni + ^{60}Ni collisions (a) and in ^{58}Ni + ^{60}Ni collisions in the side and the tip configurations (solid and dashed lines) (b).

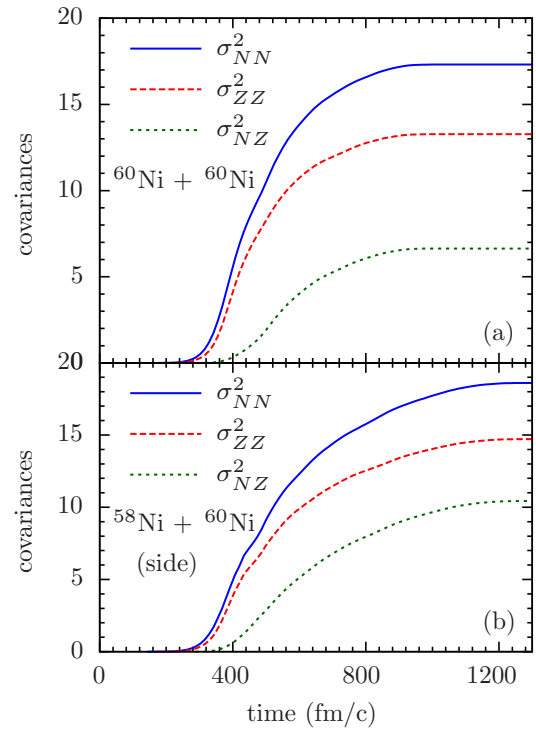

FIG. 4. Covariances in the collision of ^{60}Ni + ^{60}Ni (a) and in the collision of ^{58}Ni + ^{60}Ni in the side geometry (b) at the center of mass energy $E_{\text{c.m.}} = 135.6$ MeV and the impact parameter $b = 5.2$ fm, or equivalently initial orbital angular momentum $\ell = 73\hbar$.

partly due to the effect of the Pauli blocking of the occupied single particle states. We note that the contact time in the collision of ^{60}Ni + ^{60}Ni is about 600 fm/c, which is shorter than the contact time of about 800 fm/c in the side collision of the ^{58}Ni + ^{60}Ni system. Figure 3 shows the one-sided mean drift path at the center of mass energy $E_{\text{c.m.}} = 135.6$ MeV and the impact parameter $b = 5.2$ fm in ^{60}Ni + ^{60}Ni collisions (a) and in ^{58}Ni + ^{60}Ni collisions in the side configuration (solid line) and in the tip configuration (dashed line) (b). Here, $n = N_0 - N_1$ and $z = Z_0 - Z_1$. The quantity (N_0, Z_0) indicates the equilibrium values of neutron and proton numbers which are (32,28) for ^{60}Ni + ^{60}Ni and (31,28) for ^{58}Ni + ^{60}Ni. The quantity (N_1, Z_1) indicates the neutron and proton numbers of the fragment which are increasing due to gaining flux from its partner. Figure 4 shows the covariances in the collision of ^{60}Ni + ^{60}Ni in the upper panel (a) and in the collision of ^{58}Ni + ^{60}Ni (in the side geometry) in the lower panel (b) at the center of mass energy $E_{\text{c.m.}} = 135.6$ MeV and impact parameter $b = 5.2$ fm, or equivalently initial orbital angular momentum $\ell = 73\hbar$. Neutron-neutron σ^2_{NN}, proton-proton σ^2_{ZZ}, and neutron-proton σ^2_{NZ} covariances are indicated by solid, dashed, and dotted lines, respectively. Since for the side geometry of the ^{58}Ni + ^{60}Ni system, contact time is longer than the spherical ^{60}Ni + ^{60}Ni system, even though the center of mass energy and the impact parameters are nearly the same, the covariances are slightly larger in the ^{58}Ni + ^{60}Ni system. The mass number variance is determined as $\sigma^2_{AA} = \sigma^2_{NN} + \sigma^2_{ZZ} + 2\sigma^2_{NZ}$. In the upper panel of Fig. 5(a), we compare the result of SMF calculations (solid line) for the mass number dispersion per unit nucleon $\sigma_{MR} = \sigma_{AA}/A_T$, where A_T is the total mass number of the system, with the calculations carried out in the TDRPA (dashed line with dots) framework as a function of the impact parameters in the collision of the system ^{60}Ni + ^{60}Ni at the same center of mass energy $E_{\text{c.m.}} = 135.6$ MeV. Even though the same Skyrme force, SLy4d, is used in both calculations, the SMF calculations give up to 30% larger value than the TDRPA results for the dispersion in the impact parameter interval $b = (5.2$–$5.6)$ fm. There are two issues in relation with the results presented in Fig. 5(a). In the SMF approach the covariances are determined by solving a set of coupled differential equations given by Eqs. (17)–(19) in Ref. [55]. These coupled differential equations involve the neutron and proton diffusion coefficients and the derivatives of the drift coefficients with respect to the neutron and proton numbers of one side of the dinuclear partner around their mean values. The TDHF can only determine the evolution of the mean mass and charge asymmetries. It is not possible to calculate the derivatives of the drift coefficients with respect to the neutron and proton numbers in the TDHF description. As described in Refs. [54,55], we develop an approximate method to calculate the derivatives of the drift coefficients: We parametrize the

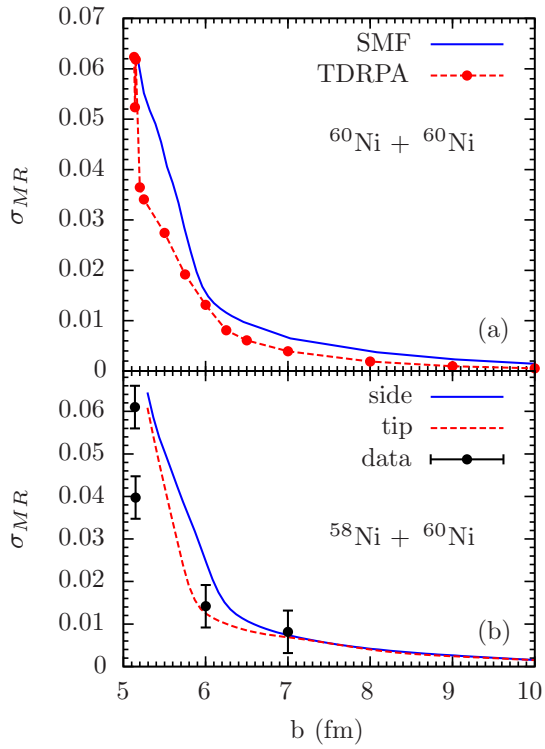

FIG. 5. Dispersion σ_{MR} per unit mass as function of the impact parameter. In (a), SMF and DRPA calculations in ^{60}Ni + ^{60}Ni collisions are indicated by solid line and dash line with dots, respectively. In (b), SMF calculations in side and tip configurations (solid and dash lines) are compared with data.

potential energy surface of the dinuclear complex in the $(N$-$Z)$ plane in terms of two parabolic forms, one of the parabolas is parallel to the valley of the stability and the other parabola is perpendicular to the stability line [54,55]. The parameters of these parabolic potential energies are determined from the mean-drift path in the case of asymmetric systems and the one-sided drift path in the cases of the symmetric systems. A great advantage of this approach, with the help of the Einstein relation, is that it provides an analytical determination of the derivatives of drift coefficients. However, in particular in the symmetric collisions, as a result of the systematic error for determining the parameters of the potential energy surface, the method may give about 10% larger reduced dispersion for small impact parameters. Currently we are trying to improve this aspect of the calculations. The second issue in Fig. 5(a) is connected with the TDRPA calculations. In the table presented in the Supplemental Material of Ref. [49], at a very small impact parameters range of $\Delta b = (5.13$–$5.25)$ fm, the reduced dispersion takes a nearly sudden drop from $\sigma_{MR} = 0.06$ to $\sigma_{MR} = 0.03$, except a large value $\sigma_{MR} = 0.06$ of the reduced dispersion at $b = 5.15$ fm, which is not indicated in Fig. 5(a). Apparently, there are also numerical issues in the TDRPA calculations at small impact parameters. The lower panel of Fig. 5(b) shows a comparison of the SMF calculations of $\sigma_{MR} = \sigma_{AA}/A_T$ for the side (solid line) and the tip (dashed line) configurations with data as a function of the impact parameters. There are four data points that are reported in Fig. 3 of Ref. [49]. These points are indicated in the figure including experimental error bars. The SMF calculations with the side configurations provide a better fit to the data. The data presented in Fig. 1 in Ref. [49] represents the cumulative mass distribution of the binary fragments. Unfolding the data to extract the reduced mass width with the help of the TDHF trajectory, in particular with small impact parameters is strongly model dependent. We believe that, in particular, the extraction of the reduced mass dispersions $\sigma_{MR} = 0.06$ and $\sigma_{MR} = 0.04$ at the nearly the same impact parameter $b = 5.20$ fm should be re-examined more carefully.

The stochastic Langevin dynamics of a set of macroscopic variables is equivalent to the Fokker-Planck description of the distribution function of the macroscopic variables [63–65]. When the driving potential energy has a parabolic form, the distribution function is a correlated Gaussian of macroscopic variables. Here, the macroscopic variable is the mass number A of a projectile-like fragment. For a given impact parameter b or the initial orbital angular momentum ℓ, the fragment mass distribution is given by a Gaussian function

$$F_\ell(A) = \frac{1}{\sqrt{2\pi}}\frac{1}{\sigma_{AA}(\ell)}\exp\left[-\frac{1}{2}\left(\frac{A - A(\ell)}{\sigma_{AA}(\ell)}\right)^2\right], \quad (1)$$

where $A(\ell)$ and $\sigma_{AA}(\ell)$ denote the mean value and the dispersion of the mass number in the collision with initial orbital angular momentum ℓ. In order to calculate the mass distribution in the collision ^{58}Ni + ^{60}Ni at center of mass energy $E_{\rm c.m.} = 135.6$ MeV, we average the Gaussian distribution given by Eq. (1) over a range of initial orbital angular momentum $\ell_0 \leqslant \ell \leqslant \ell_m$, where $\ell_0 = 73\hbar$ is the lowest initial orbital which does not lead to fusion and $\ell_m = 96\hbar$ is the maximum angular momentum corresponding to the detector resolution limit. The mass distribution of the primary fragment is given by the weighted average of the Gaussian functions

$$P(A) = \frac{\eta}{\sum_\ell (2\ell+1)}\sum_\ell (2\ell+1)F_\ell(A)\,, \quad (2)$$

where η is a normalization constant. The solid and dashed lines in Fig. 6 show the yield obtained from the SMF calculations which are averaged over the tip and side configurations. The experimental data are indicated by the dotted line. Since the system is very close to symmetry, the mass asymmetry reaches the equilibrium value in a very short time interval. In Eq. (2) we take the equilibrium value $A = 59$ for each initial orbital angular momentum in the interval where the summation is carried out. We determined the normalization constant η by matching the peak value of the experimental yield at $A = 59$ by matching the peak value of the experimental yield at $A = 59$. The experimental yield indicated by the dotted line, is deduced from part (a) of Fig. 1 in Ref. [49] with the data taken at the energy $E_{\rm c.m.}/V_B = 1.4$. In order to check the sensitivity of the range of impact parameters on the fragment cumulative yield, we carry out the calculation of Eq. (2) for the cumulative yield by taking the upper limit of the range of the initial angular momentum as $\ell_m = 90\hbar$. The result is shown by dashed line in Fig. 6, and we observe no appreciable difference in the integrated mass yield. In the calculation of

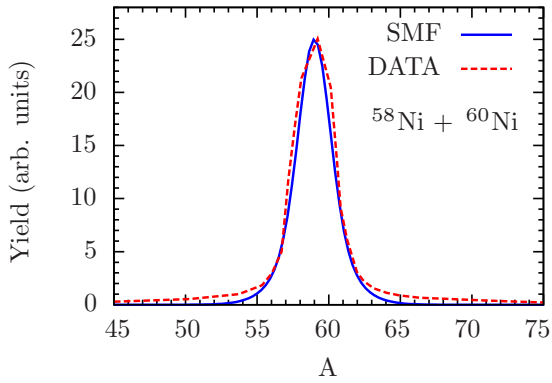

FIG. 6. Solid and dashed lines are the yields obtained from the SMF calculations, which are averaged over the tip and side configurations. For SMF1 and SMF2, the upper limit of the initial angular momentum is taken as $\ell_m = 96\hbar$ and $\ell_m = 90\hbar$, respectively. The experimental yield is indicated by the dotted line.

the integrated yield, we employ a sharp cut off approximation. We determine the critical angular momentum $\ell_0 = 73\hbar$ for fusion from the TDHF calculations, and assume multinucleon exchange occurs above this critical angular momentum. In principal transition should take place smoothly from fusion to the multinucleon transfer process. If the SMF calculations are carried out by generating an ensemble of events, it should be possible to observe partial transition from fusion to the multinucleon transfer process. However, in the present diffusion approach, it is not possible to describe the smooth transition from fusion to the multinucleon transfer mechanism.

IV. CONCLUSIONS

In conclusion, we find that the quantal diffusion description deduced from the SMF approach provides a good description for the fragment mass distribution observed in ^{58}Ni + ^{60}Ni collisions at the center of mass energy $E_{\text{c.m.}} = 135.6$ MeV without any adjustable parameters except the parameters of the effective Skyrme interaction in the TDHF code. Since in the small impact parameter range, the mass dispersions take rather large values, the partition of the integrated data into small impact parameter range may introduce large experimental errors. The sizable discrepancy between the SMF calculations and the data from part (b) of Fig. 5 may arise from such partitioning of the integrated experimental data, in particular in the small impact parameter range.

ACKNOWLEDGMENTS

S.A. gratefully acknowledges the IPN-Orsay and the Middle East Technical University for the warm hospitality extended to him during his visits. S.A. also gratefully acknowledges useful discussions with D. Lacroix, and is very much thankful to F. Ayik for continuous support and encouragement. This work is supported in part by US DOE Grants No. DE-SC0015513 and No. DE-SC0013847, and in part by TUBITAK Grant No. 117F109.

[1] Ph. Chomaz, M. Di Toro, and A. Smerzi, Pre-equilibrium effects on properties of hot giant-dipole resonances, Nucl. Phys. A **563**, 509 (1993).
[2] C. H. Dasso, G. Pollarolo, and A. Winther, Particle evaporation following multinucleon transfer processes with radioactive beams, Phys. Rev. C **52**, 2264 (1995).
[3] S. Flibotte, Ph. Chomaz, M. Colonna, M. Cromaz, J. DeGraaf, T. E. Drake, A. Galindo-Uribarri, V. P. Janzen, J. Jonkman, S. W. Marshall, S. M. Mullins, J. M. Nieminen, D. C. Radford, J. L. Rodriguez, J. C. Waddington, D. Ward, and J. N. Wilson, Pre-Equilibrium Effects in the Population of Giant Dipole Resonances, Phys. Rev. Lett. **77**, 1448 (1996).
[4] V. Baran, D. M. Brink, M. Colonna, and M. Di Toro, Collective Dipole Bremsstrahlung in Fusion Reactions, Phys. Rev. Lett. **87**, 182501 (2001).
[5] C. Simenel, Ph. Chomaz, and G. de France, Quantum Calculation of the Dipole Excitation in Fusion Reactions, Phys. Rev. Lett. **86**, 2971 (2001).
[6] B. B. Back, H. Esbensen, C. L. Jiang, and K. E. Rehm, Recent developments in heavy-ion fusion reactions, Rev. Mod. Phys. **86**, 317 (2014).
[7] R. A. Broglia, C. H. Dasso, S. Landowne, and A. Winther, Possible effect of transfer reactions on heavy ion fusion at sub-barrier energies, Phys. Rev. C **27**, 2433(R) (1983).
[8] H. Esbensen and S. Landowne, Coupled-channels calculations for transfer reactions, Nucl. Phys. A **492**, 473 (1989).
[9] C. R. Morton, M. Dasgupta, D. J. Hinde, J. R. Leigh, R. C. Lemmon, J. P. Lestone, J. C. Mein, J. O. Newton, H. Timmers, N. Rowley, and A. T. Kruppa, Clear Signatures of Specific Inelastic and Transfer Channels in the Distribution of Fusion Barriers, Phys. Rev. Lett. **72**, 4074 (1994).
[10] H. Timmers, D. Ackermann, S. Beghini, L. Corradi, J. H. He, G. Montagnoli, F. Scarlassara, A. M. Stefanini, and N. Rowley, A case study of collectivity, transfer and fusion enhancement, Nucl. Phys. A **633**, 421 (1998).
[11] A. M. Stefanini, B. R. Behera, S. Beghini, L. Corradi, E. Fioretto, A. Gadea, G. Montagnoli, N. Rowley, F. Scarlassara, S. Szilner, and M. Trotta, Sub-barrier fusion of ^{40}Ca + ^{94}Zr: Interplay of phonon and transfer couplings, Phys. Rev. C **76**, 014610 (2007).
[12] V. I. Zagrebaev, Sub-barrier fusion enhancement due to neutron transfer, Phys. Rev. C **67**, 061601(R) (2003).
[13] V. Zagrebaev and W. Greiner, Low-energy collisions of heavy nuclei: dynamics of sticking, mass transfer and fusion, J. Phys. G **34**, 1 (2007).
[14] A. S. Umar, V. E. Oberacker, and J. A. Maruhn, Neutron transfer dynamics and doorway to fusion in time-dependent Hartree-Fock theory, Eur. Phys. J. A **37**, 245 (2008).
[15] L. Corradi, G. Pollarolo, and S. Szilner, Multinucleon transfer processes in heavy-ion reactions, J. Phys. G **36**, 113101 (2009).
[16] H. Q. Zhang, C. J. Lin, F. Yang, H. M. Jia, X. X. Xu, Z. D. Wu, F. Jia, S. T. Zhang, Z. H. Liu, A. Richard, and C. Beck, Near-barrier fusion of ^{32}S + ^{90,96}Zr: The effect of multi-neutron transfers in sub-barrier fusion reactions, Phys. Rev. C **82**, 054609 (2010).

[17] Z. Kohley, J. F. Liang, D. Shapira, R. L. Varner, C. J. Gross, J. M. Allmond, A. L. Caraley, E. A. Coello, F. Favela, K. Lagergren, and P. E. Mueller, Near-Barrier Fusion of Sn + Ni and Te + Ni Systems: Examining the Correlation Between Nucleon Transfer and Fusion Enhancement, Phys. Rev. Lett. **107**, 202701 (2011).

[18] G. Montagnoli, A. M. Stefanini, H. Esbensen, C. L. Jiang, L. Corradi, S. Courtin, E. Fioretto, A. Goasduff, J. Grebosz, F. Haas, M. Mazzocco, C. Michelagnoli, T. Mijatovic, D. Montanari, C. Parascandolo, K. E. Rehm, F. Scarlassara, S. Szilner, X. D. Tang, and C. A. Ur, Effects of transfer channels on near- and sub-barrier fusion of ^{3}S + ^{48}Ca, Phys. Rev. C **87**, 014611 (2013).

[19] M. S. Gautam, Role of neutron transfer in the enhancement of sub-barrier fusion excitation functions of various systems using an energy-dependent Woods-Saxon potential, Phys. Rev. C **90**, 024620 (2014).

[20] D. Bourgin, S. Courtin, F. Haas, A. M. Stefanini, G. Montagnoli, A. Goasduff, D. Montanari, L. Corradi, E. Fioretto, J. Huiming, F. Scarlassara, N. Rowley, S. Szilner, and T. Mijatović, Barrier distributions and signatures of transfer channels in the ^{40}Ca + ^{58,64}Ni fusion reactions at energies around and below the Coulomb barrier, Phys. Rev. C **90**, 044610 (2014).

[21] J. F. Liang, J. M. Allmond, C. J. Gross, P. E. Mueller, D. Shapira, R. L. Varner, M. Dasgupta, D. J. Hinde, C. Simenel, E. Williams, K. Vo-Phuoc, M. L. Brown, I. P. Carter, M. Evers, D. H. Luong, T. Ebadi, and A. Wakhle, Examining the role of transfer coupling in sub-barrier fusion of ^{46,50}Ti + ^{124}Sn, Phys. Rev. C **94**, 024616 (2016).

[22] V. V. Volkov, Deep inelastic transfer reactions—The new type of reactions between complex nuclei, Phys. Rep. **44**, 93 (1978).

[23] N. V. Antonenko and R. V. Jolos, The microscopic treatment of proton and neutron multiple transfer in DIC, Z. Phys. A **338**, 423 (1991).

[24] G. G. Adamian, N. V. Antonenko, and W. Scheid, Characteristics of quasifission products within the dinuclear system model, Phys. Rev. C **68**, 034601 (2003).

[25] Y. Aritomo, Analysis of dynamical processes using the mass distribution of fission fragments in heavy-ion reactions, Phys. Rev. C **80**, 064604 (2009).

[26] A. S. Umar, V. E. Oberacker, and C. Simenel, Fusion and quasifission dynamics in the reactions ^{48}Ca + ^{249}Bk and ^{50}Ti + ^{249}Bk using a time-dependent Hartree-Fock approach, Phys. Rev. C **94**, 024605 (2016).

[27] M. Evers, M. Dasgupta, D. J. Hinde, D. H. Luong, R. Rafiei, R. du Rietz, and C. Simenel, Cluster transfer in the reaction ^{16}O + ^{208}Pb at energies well below the fusion barrier: A possible doorway to energy dissipation, Phys. Rev. C **84**, 054614 (2011).

[28] K. Washiyama and D. Lacroix, Energy dissipation in fusion reactions from dynamical mean-field theory, Int. J. Mod. Phys. E **18**, 2114 (2009).

[29] V. E. Oberacker, A. S. Umar, and C. Simenel, Dissipative dynamics in quasifission, Phys. Rev. C **90**, 054605 (2014).

[30] A. S. Umar, C. Simenel, and W. Ye, Transport properties of isospin asymmetric nuclear matter using the time-dependent Hartree-Fock method, Phys. Rev. C **96**, 024625 (2017).

[31] Kai Wen, M. C. Barton, Arnau Rios, and P. D. Stevenson, Two-body dissipation effect in nuclear fusion reactions, Phys. Rev. C **98**, 014603 (2018).

[32] G. G. Adamian, R. V. Jolos, A. K. Nasirov, and A. I. Muminov, Effects of shell structure and N/Z ratio of a projectile on the excitation energy distribution between interacting nuclei in deep-inelastic collisions, Phys. Rev. C **53**, 871 (1996).

[33] Y. Aritomo, Fusion hindrance and roles of shell effects in superheavy mass region, Nucl. Phys. A **780**, 222 (2006).

[34] V. Zagrebaev and W. Greiner, Shell effects in damped collisions: A new way to superheavies, J. Phys. G **34**, 2265 (2007).

[35] E. M. Kozulin, G. N. Knyazheva, I. M. Itkis, N. I. Kozulina, T. A. Loktev, K. V. Novikov, and I. Harca, Shell effects in fission, quasifission and multinucleon transfer reaction, J. Phys. Conf. Ser. **515**, 012010 (2014).

[36] G. Mohanto, D. J. Hinde, K. Banerjee, M. Dasgupta, D. Y. Jeung, C. Simenel, E. C. Simpson, A. Wakhle, E. Williams, I. P. Carter, K. J. Cook, D. H. Luong, C. S. Palshetkar, and D. C. Rafferty, Interplay of spherical closed shells and N/Z asymmetry in quasifission dynamics, Phys. Rev. C **97**, 054603 (2018).

[37] A. S. Umar, V. E. Oberacker, and C. Simenel, Shape evolution and collective dynamics of quasifission in the time-dependent Hartree-Fock approach, Phys. Rev. C **92**, 024621 (2015).

[38] C. Simenel, Nuclear quantum many-body dynamics, Eur. Phys. J. A **48**, 152 (2012).

[39] C. Simenel and A. S. Umar, Heavy-ion collisions and fission dynamics with the time-dependent Hartree-Fock theory and its extensions, Prog. Part. Nucl. Phys. (2018), doi:10.1016/j.ppnp.2018.07.002.

[40] C. Simenel, Particle Transfer Reactions with the Time-Dependent Hartree-Fock Theory Using a Particle Number Projection Technique, Phys. Rev. Lett. **105**, 192701 (2010).

[41] C. Simenel, Particle-Number Fluctuations and Correlations in Transfer Reactions Obtained Using the Balian-Vénéroni Variational Principle, Phys. Rev. Lett. **106**, 112502 (2011).

[42] Guillaume Scamps and Denis Lacroix, Effect of pairing on one- and two-nucleon transfer below the Coulomb barrier: A time-dependent microscopic description, Phys. Rev. C **87**, 014605 (2013).

[43] G. Scamps, V. V. Sargsyan, G. G. Adamian, N. V. Antonenko, and D. Lacroix, Analysis of the dependence of the few-neutron transfer probability on the Q-value magnitudes, Phys. Rev. C **91**, 024601 (2015).

[44] G. Scamps and Y. Hashimoto, Transfer probabilities for the reactions ^{14,20}O + ^{20}O in terms of multiple time-dependent Hartree-Fock-Bogoliubov trajectories, Phys. Rev. C **96**, 031602(R) (2017).

[45] K. Sekizawa and K. Yabana, Time-dependent Hartree-Fock calculations for multinucleon transfer processes in ^{40,48}Ca + ^{124}Sn, ^{40}Ca + ^{208}Pb, and ^{58}Ni + ^{208}Pb reactions, Phys. Rev. C **88**, 014614 (2013).

[46] K. Sekizawa and K. Yabana, Particle-number projection method in time-dependent Hartree-Fock theory: Properties of reaction products, Phys. Rev. C **90**, 064614 (2014).

[47] K. Sekizawa and K. Yabana, Time-dependent Hartree-Fock calculations for multinucleon transfer and quasifission processes in the ^{64}Ni + ^{238}U reaction, Phys. Rev. C **93**, 054616 (2016).

[48] K. Sekizawa, Enhanced nucleon transfer in tip collisions of ^{238}U + ^{124}Sn, Phys. Rev. C **96**, 041601(R) (2017).

[49] E. Williams, K. Sekizawa, D. J. Hinde, C. Simenel, M. Dasgupta, I. P. Carter, K. J. Cook, D. Y. Jeung, S. D. McNeil, C. S. Palshetkar, D. C. Rafferty, K. Ramachandran,

and A. Wakhle, Exploring Zeptosecond Quantum Equilibration Dynamics: From Deep-Inelastic to Fusion-Fission Outcomes in ^{58}Ni + ^{60}Ni Reactions, Phys. Rev. Lett. **120**, 022501 (2018).

[50] R. Balian and M. Vénéroni, Fluctuations in a time-dependent mean-field approach, Phys. Lett. B **136**, 301 (1984).

[51] J. M. A. Broomfield and P. D. Stevenson, Mass dispersions from giant dipole resonances using the Balian-Vénéroni variational approach, J. Phys. G **35**, 095102 (2008).

[52] J. M. A. Broomfield, Calculations of mass distributions using the Balian-Vénéroni variational approach, Ph.D. thesis, University of Surrey, 2009.

[53] S. Ayik, A stochastic mean-field approach for nuclear dynamics, Phys. Lett. B **658**, 174 (2008).

[54] S. Ayik, B. Yilmaz, O. Yilmaz, A. S. Umar, and G. Turan, Multinucleon transfer in central collisions of ^{238}U + ^{238}U, Phys. Rev. C **96**, 024611 (2017).

[55] S. Ayik, B. Yilmaz, O. Yilmaz, and A. S. Umar, Quantal diffusion description of multinucleon transfers in heavy-ion collisions, Phys. Rev. C **97**, 054618 (2018).

[56] D. Lacroix and S. Ayik, Stochastic quantum dynamics beyond mean field, Eur. Phys. J. A **50**, 95 (2014).

[57] W. U. Schröder, J. R. Huizenga, and J. Randrup, Correlated mass and charge transport induced by statistical nucleon exchange in damped nuclear reactions, Phys. Lett. B **98**, 355 (1981).

[58] A. C. Merchant and W. Nörenberg, Neutron and proton diffusion in heavy-ion collisions, Phys. Lett. B **104**, 15 (1981).

[59] A. C. Merchant and W. Nörenberg, Microscopic transport theory of heavy-ion collisions, Z. Phys. A **308**, 315 (1982).

[60] A. S. Umar, M. R. Strayer, J.-S. Wu, D. J. Dean, and M. C. Güçlü, Nuclear Hartree-Fock calculations with splines, Phys. Rev. C **44**, 2512 (1991).

[61] A. S. Umar and V. E. Oberacker, Three-dimensional unrestricted time-dependent Hartree-Fock fusion calculations using the full Skyrme interaction, Phys. Rev. C **73**, 054607 (2006).

[62] K.-H. Kim, T. Otsuka, and P. Bonche, Three-dimensional TDHF calculations for reactions of unstable nuclei, J. Phys. G **23**, 1267 (1997).

[63] H. Risken and T. Frank, *The Fokker–Planck Equation* (Springer-Verlag, Berlin, 1996).

[64] C. W. Gardiner, *Quantum Noise* (Springer-Verlag, Berlin, 1991).

[65] U. Weiss, *Quantum Dissipative Systems*, 2nd ed. (World Scientific, Singapore, 1999).